Impact of phonons on quantum phase transitions in nanorings of coupled quantum dots

Ioan Bâldea,[1,2,*] Horst Köppel,[1] and Lorenz S. Cederbaum[1]
[1]*Theoretische Chemie, Physikalisch-Chemisches Institut, Universität Heidelberg, INF 229, D-69120 Heidelberg, Germany*
[2]*Physikalisches Institut, Universität Karlsruhe, D-76129 Karlsruhe, Germany*
(Received 30 June 2003; revised manuscript received 3 November 2003; published 17 February 2004)

CDW-to-CDW and CDW-to-SDW (CDW/SDW=charge-spin-density wave) quantum phase transitions have been recently reported for finite rings described by an extended Hubbard model [I. Bâldea, H. Köppel, and L. S. Cederbaum, Eur. Phys. J. B **20**, 289 (2001)]. We present exact (Lanczos) diagonalization results which demonstrate that these transitions survive in the presence of a *dynamic* Su-Schrieffer-Heeger (SSH) electron-phonon coupling. The two transitions are affected in a different way discussed in detail. By treating the SSH electron-phonon coupling dynamically, two levels of different symmetries do cross, allowing one to define precisely a critical point. Because the ground-state symmetry changes at the critical points, we suggest to study the quantum phase transitions by optical methods. Molecular rings such as polyenes (annulenes) turn out to be too far from the critical points, where the most interesting phenomena occur. However, we present an analysis revealing that, if metallic quantum dots of the type already fabricated can be assembled in nanorings, model parameters can be tuned and quantum phase transitions can become observable.

DOI: 10.1103/PhysRevB.69.075307 PACS number(s): 73.40.Gk, 71.45.Lr, 73.23.−b

I. INTRODUCTION

Extended Hubbard models,[1] often supplemented by electron-phonon couplings, provide a very popular framework for studying strongly correlated systems. Their ground-state can be characterized by a variety of correlations, such as charge-density, spin-density, bond-order waves (CDW, SDW, BOW, respectively), or charge separation. Since these models are not exactly solvable analytically even in the absence of phonons, exact results obtained numerically for finite clusters are very desirable.

To study clusters consisting of a small number of units ($N\sim 10$), exact numerical (Lanczos) diagonalization is most useful because it allows one to compute eigenvectors directly, thus providing the richest physical information, to discriminate (lowest) excitations, even if they possess different symmetries and/or are almost degenerate, and to compute frequency-dependent responses. Other numerical [e.g., density-matrix renormalization group (DMRG),[2] Monte Carlo[3]] methods could handle larger systems in the ground-state, but difficulties arise, e.g., when dealing with frequency-dependent responses.

While exact diagonalization approaches of infinite solids are inherently confronted with problems of extrapolations, they can be employed directly to nanostructures consisting of a small number of quantum dots (QD's). QD's behave like artificial atoms;[4] being confined within a few nanometers, electrons occupy quantized levels analogous to atomic orbitals in ordinary atoms. Advances in nanotechnologies allow one to fabricate assemblies of metallic[5–7] and semiconducting[8] QD's, or ''artificial'' molecules.[9] Most electrons are localized on individual QD's. However, a small number of (''valence'') electrons are bound weakly enough to become delocalized over the whole ''molecule'' if the overlap of their wave functions for adjacent QD's is sufficiently large. The salient feature of such artificial atoms and molecules is that, unlike the natural counterparts, their properties can be tuned by varying the dot diameter $2R$ and/or interdot spacing D. Individual QD's can be characterized by the on-site Coulomb repulsion energy U (related to the QD self-elastance) and the energy of valence electrons ϵ. QD's are coupled by electron tunneling (resonance integral t_0) and Coulomb interaction V (related to the mutual elastance). U and ϵ (mainly) depend on R, whereas t_0 and V depend on D. Previously, the extended Hubbard model has been used for studying transport in arrays of semiconducting QD's (Ref. 10) and disorder effects in metallic QD arrays.[11]

In view of their tunable properties, assemblies of QD's can be used to study many aspects unexplored so far for interacting electron systems. For instance, they can be continuously driven from a weak correlation regime to strong correlation regime. To this aim, one can monitor ionization, as demonstrated recently by two of us.[12] An interesting problem that can be studied in view of the tunability is the phase diagram for mesoscopic rings in the presence of strong electronic correlations. This has been demonstrated by our recent studies,[13] revealing that finite rings possess a phase diagram richer than for infinite ones. What makes the difference from infinite systems is the symmetry of an exact eigenstate (e.g., ground-state), which cannot be broken in finite ones. In the latter case, the *collective* electronic tunneling between multielectronic configurations that are classically equivalent restores the symmetry and enriches the phase diagram. The phase diagram comprises, besides critical lines related to quantum phase transitions that are also possible in infinite systems (e.g. CDW-to-SDW transition), new critical lines, specific for mesoscopic systems, related to tunneling-driven quantum phase transitions. The former critical lines separate states characterized by different orderings and symmetries, while the latter separate states with the same ordering, but with different symmetries (e.g. CDW-to-CDW transitions); see Ref. 13 for details.

In the present paper, we shall extend our previous studies[13] on finite rings by incorporating a *dynamic* coupling

of electrons to phonons of Su-Schrieffer-Heeger (SSH) type[14] into the extended Hubbard model. From a general theoretical standpoint, it is interesting to address the question whether the tunneling-driven quantum phase transitions of Ref. 13 survive the quantum phonon fluctuations. The SSH electron-phonon coupling is important in real systems; for instance, it is responsible for dimerization in cyclic polyenes[15] and polyacetylene.[14] SSH phonons may also be important for nanorings of QD's, once nanotechnologies are able to fabricate (almost) identical QD's forming (almost) perfect regular arrays. The interdot spacing D is a dynamical variable, since QD's are not rigidly fixed on the substrate. Because of difficulties related to the infinite phonon Hilbert space, theoretical studies on dynamic phonons by exact or almost exact numerical methods have appeared only recently.[16–20] Except for Ref. 17, which also considered the optical conductivity, these studies restricted themselves to the ground-state or at most to a few of the lowest excitations.

The remaining part of this paper is organized as follows. In Sec. II, we specify the model and discuss its symmetries. Then, we present a variety of general properties, with emphasis on those specific for mesoscopic systems. They refer to the ground-state (Sec. III) and lower excited states (Sec. IV), as well as optical absorption (Sec. V). In Sec. III C, results obtained by treating the dynamic electron-phonon coupling are compared to those for a classically deformable lattice. Some discussions and conclusions make the object of the final Sec. VI.

II. MODEL

The system under consideration is a collection of an even number N of sites (QD's) placed on a nanoring. A QD is modeled by a single spin-1/2 ''atomic'' orbital occupied by one electron (half-filling case). The Hamiltonian reads

$$H=\sum_{l=1}^{N}\sum_{\sigma=\uparrow,\downarrow}\left[-t_0+(-1)^l\frac{g}{\sqrt{N}}(b+b^\dagger)\right]\times(a_{l,\sigma}^\dagger a_{l+1,\sigma}+a_{l+1,\sigma}^\dagger a_{l,\sigma})+\sum_{l=1}^{N}\epsilon n_l+\sum_{l=1}^{N}(Un_{l,\uparrow}n_{l,\downarrow}+Vn_ln_{l+1})+\Omega(b^\dagger b+1/2). \quad (1)$$

Here, a ($a^\dagger$) and b ($b^\dagger$) denote annihilation (creation) operators for electrons and phonons, respectively, $n_{l,\sigma}\equiv a_{l,\sigma}^\dagger a_{l,\sigma}$, $n_l\equiv n_{l,\uparrow}+n_{l,\downarrow}$, t_0 is the nearest-neighbor hopping integral, and Ω is the bare phonon frequency. In addition to the electronic Hubbard U and V terms, Eq. (1) includes the coupling of electrons to SSH phonons,[14] characterized below by the dimensionless strength $\gamma\equiv g/\sqrt{\Omega t_0/2}$. We consider identical sites and set site energies $\epsilon=0$.

We shall consider open-shell systems because the phase diagram turned out to be richer in this case.[13] Open-shell situations correspond to periodic rings with $N=4\kappa$ and to antiperiodic rings with $N=4\kappa+2$ (κ is an integer).[21] The difference between the highest occupied and the lowest unoccupied single-electron levels (HOMO-LUMO gap,) vanishes only in the two aforementioned cases. A vanishing HOMO-LUMO gap mimics the divergent electronic density of states at the Fermi level of an infinite system which is responsible, e.g., for the *finite* static lattice dimerization for arbitrarily small γ. Otherwise, although decreasing as $1/N$, this gap remains finite and the dimerization requires a minimum value of γ;[22,23,18] then, it would be hard to make this gap much smaller than other realistic model parameters at sizes for which the exact diagonalization can be done. Therefore, by considering below open-shell situations, we argue that the results derived for small clusters (here, up to $N=12$) should also have relevance for larger systems and, to a certain extent, for infinite systems.[24]

Similar to the case where phonons are absent,[13] the symmetry of the Hamiltonian (1) is important for the eigenstate classification. One can easily show that the spatial symmetry group of Eq. (1) is $\mathbf{C}_{\mathcal{N},v}$ ($\mathcal{N}=N$ for periodic boundaries and $\mathcal{N}=2N$ for antiperiodic boundaries), comprising rotations $\mathbf{T}_k\equiv\mathbf{T}^k$ [$a_{l,\sigma}\rightarrow a_{l+k,\sigma}$ and $Q\rightarrow(-1)^kQ$] around a principal axis $\mathcal{C}_N$ as well as two distinct classes of reflection planes perpendicular to $\mathcal{C}_N$, $\mathbf{m}_v(j)$ ($a_{l,\sigma}\rightarrow a_{N+2j-l,\sigma}$, $Q\rightarrow -Q$) and $\mathbf{m}_d(j)$ ($a_{l,\sigma}\rightarrow a_{N+1+2j-l,\sigma}$, $Q\rightarrow Q$). Here, $0\leqslant k\leqslant\mathcal{N}-1$, $0\leqslant j\leqslant\mathcal{N}/2-1$, and Q is the dimerization coordinate ($b\sqrt{2}=Q+\partial/\partial Q$, $b^\dagger\sqrt{2}=Q-\partial/\partial Q$). Further symmetries of the Hamiltonian (1) are the particle-hole transformation $\mathbf{P}$ [$a_{l,\sigma}\rightarrow(-1)^l a_{l,\sigma}^\dagger$, $Q\rightarrow Q$] and the spin flip $\mathbf{F}$ ($a_{l,\sigma}\rightarrow a_{l,-\sigma}$, $Q\rightarrow Q$). *No* symmetry breaking is possible in finite rings, unlike in infinite ones. Consequently, under the aforementioned transformations, the nondegenerate eigenstates $|\Psi_\alpha\rangle$ of Eq. (1) should be of either even ($|\Psi_\alpha\rangle\rightarrow+|\Psi_\alpha\rangle$) or odd ($|\Psi_\alpha\rangle\rightarrow-|\Psi_\alpha\rangle$) parity. The corresponding eigenvalues (±1) of the operators $\mathbf{T}$, $\mathbf{P}$, $\mathbf{F}$, $\mathbf{m}_v(0)$, and $\mathbf{m}_d(0)$ will be denoted by $\mathcal{T}$, $\mathcal{P}$, $\mathcal{F}$, m_v, and m_d, respectively. Although certain symmetries of electron-phonon models similar to Eq. (1) relevant for infinite systems have been discussed previously (e.g., Ref. 25), to our knowledge, a full classification along these lines has not been given before in the literature.

The results presented below have been obtained by means of exact (Lanczos) diagonalization. For specific details on this method see, e.g., Refs. 17, 18, and 13, and citations therein.

III. GROUND-STATE PROPERTIES

A. Considerations on quantum phase transitions in nanorings

As discussed previously,[13] quantum phase transitions can occur at zero temperature ($T=0$) in commensurate mesoscopic rings of strongly correlated electrons due to quantum fluctuations, analogous to traditional phase transitions caused by thermal fluctuations. Quantum phase transitions can be observed by varying model parameters. Studying quantum phase transitions in this way is inconceivable in ordinary solids or molecules, but is possible in nanorings, as we suggest below by referring to recent achievements in the fabrication of arrays of metallic QD's. Recently, it became possible to assemble narrow size distributions ($\sim 5\%$) of silver QD's with diameter ($2R$) of a few nanometers in hexagonal

arrays.[5–7] The interdot separation D (measured between QD centers) has been nearly continuously varied in the range $1.1 \lesssim D/(2R) \lesssim 1.8$, allowing a wide tuning of various physical properties.[5–7] This is mainly due to the exponential behavior found for $t_0[\propto \exp(-2.75D/R)]$,[11] as in polyenes.[15] In the above range, t_0 changes by a factor ~ 50. For $D/(2R)=1.2$, a value $t_0=0.5$ eV has been extracted by fitting experimental data.[27]

For Ag QD's with $2R \approx 2.6$ nm, Coulomb blockade experiments, using scanning tunneling microscopy, led to $U=0.34$ eV.[7] This value agrees with the estimate $U=e^2/(\varepsilon_r R)$ deduced by assuming a spheric QD (ε_r is dielectric constant of surrounding material).[7,6,26] Obviously, the above formula represents a crude approximation even within the classical spherical model; it corresponds to a metallic charged spherical grain embedded in an infinite dielectric medium. Assuming the passivating ligand surrounding the metallic dot as a spherical shell of outer radius ρ, one gets an enhanced on-site repulsion by a factor $U'/U=1+(\varepsilon_r-1)R/\rho$. From intuitive reasons, one could expect that the Coulomb repulsion between adjacent sites V is weaker than the on-site repulsion U. A precise formula for V is not documented. For the observability of the presently discussed quantum phase transitions [see Fig. 1(a) and the discussion below], large enough values of V/U are of interest, corresponding to QD's very close to each other.

For this case, one can estimate $V/U \approx v/u$ classically, as the ratio between the mutual- and self-elastances (v and u, respectively) of two identical spheres in a homogeneous medium.[12] Results for u and v deduced numerically by using classical electrostatics are presented in Fig. 1(b).[28] Along with the aforementioned behavior of t_0, these u and v curves suggest that, by varying D/R, wide regions of the phase diagram [Fig. 1(a)] can be explored.

A comment is in order at this point. Before considering nanorings of quantum dots, we have investigated whether cyclic molecules may correspond to points of the phase diagram close enough to the critical lines. To this aim, we have examined in detail cyclic polyenes C_NH_N. As is well known, the Pariser-Parr-Pople model,[29] the counterpart of the extended Hubbard model in the chemical area, was originally introduced just to describe π electrons of these molecules. By adjusting only four parameters (U, V, Ω, and γ) of model (1) one can reproduce an impressive amount of reliable experimental and *ab initio* data of smaller molecules — benzene (C_6H_6), cyclobutadiene (C_4H_4), and cyclooctatetraene (C_8H_8) — as well as for polyacetylene: ground-state properties (e.g., dimerization amplitude), photoionization, as well as (singlet and triplet) electronic and phononic excitations.[30] The related technical details will be presented elsewhere, since they heavily rely on chemical and molecular physics. Here we only note that the value $V/U=0.28$ found in this way[30] is too far from the critical lines of the phase diagram [see Fig. 1(a)]. Therefore, no precursor effects of the quantum phase transitions discussed in this paper could be expected in polyenes.

Below, we shall first present the phase diagram of interacting electrons in (nano)rings obtained by exact (Lanczos) diagonalization in the absence of phonons. Then, we shall show how the quantum phase transitions occurring in the purely electronic system are affected by the coupling of electrons to SSH phonons.

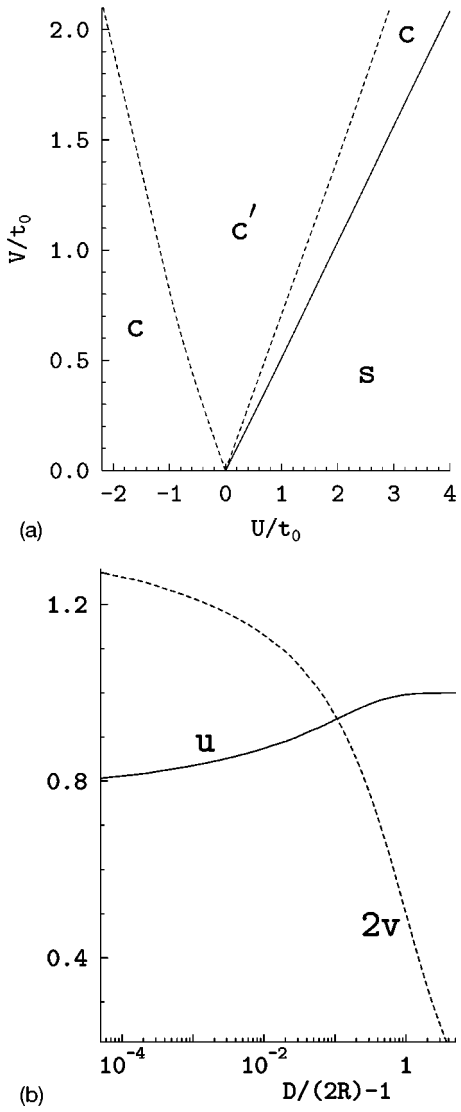

FIG. 1. (a) Phase diagrams for 12-site periodic rings. The dashed critical lines separate the parameter space into CDW phases c and c' with different *symmetries*. The phases c and s separated by the solid line differ both in orderings (CDW and SDW, respectively) and symmetries. (b) Self- and mutual elastances (u and v, respectively) obtained within classical electrostatics for two identical spheres of radius R whose centers are separated by a distance D. They are normalized to the elastance ($1/R$) of an isolated sphere. The ratio v/u represents the classical approximation of V/U. The equality $u=2v$ holds for $D/(2R)=1.107$.

A critical point of a quantum phase transition is defined by the intersection of levels corresponding to the lowest eigenstates with different correlations and/or symmetries.[13] In Fig. 1(a), we present the phase diagram for periodic 12-site rings and $V \geqslant 0$ in the absence of electron-phonon coupling, obtained by level crossing.[13,31] One should note that below we mainly refer to the case $N=12$ since this is the

largest size we can study by exact diagonalization in the presence of phonons. However, it is worth emphasizing that the results for smaller rings are analogous, as one can see by comparing the present results without phonons to those for smaller sizes we reported recently.[13] Similar to smaller rings ($N=6,8,10$),[13] the ground-state phase diagram for $N=12$ [Fig. 1(a)] comprises two CDW regions (phases c and c'), where CDW correlations dominate over SDW correlations, and one SDW region (phase s), where SDW correlations dominate over CDW ones. Both states c and c' represent CDW phases, but their symmetries are different; more precisely, they have the symmetries of the symmetric and antisymmetric superpositions $|\mathrm{CDW}_1\rangle \pm |\mathrm{CDW}_2\rangle$, respectively, each term representing one of the two classically equivalent CDWs in the bipolaronic limit. In occupation number representation, $|\mathrm{CDW}_1\rangle = |\cdots 0202\cdots\rangle$ and $|\mathrm{CDW}_2\rangle = |\cdots 2020\cdots\rangle$. The state s corresponds to a SDW phase with the symmetries of the superposition $|\mathrm{SDW}_1\rangle + |\mathrm{SDW}_2\rangle$ of the two classically equivalent SDWs in the antiferromagnetic limit, $|\mathrm{SDW}_1\rangle = |\cdots\uparrow\downarrow\uparrow\downarrow\cdots\rangle$ and $|\mathrm{SDW}_2\rangle = |\cdots\downarrow\uparrow\downarrow\uparrow\cdots\rangle$.[32] The symmetries of the state c are $\mathcal{T}=m_d=m_v=+1$ (irreducible representation $^1A_1$ of the point group $C_{12,v}$), and $\mathcal{P}=\mathcal{F}=+1$; for the state c', $\mathcal{T}=m_d=-1, m_v=+1$ (irreducible representation $^1B_1$), $\mathcal{P}=-1$, and $\mathcal{F}=+1$. The symmetries of the SDW-type state s are $\mathcal{T}=m_v=-1$, $m_d=+1$ (irreducible representation $^1B_2$), and $\mathcal{P}=\mathcal{F}=+1$. In Fig. 1(a), the lines between the phases c and c' correspond to a CDW-to-CDW quantum phase transition, the line between c and s corresponds to a CDW-to-SDW quantum phase transition.

Similar to the case without phonons, one can determine a ground-state phase diagram by crossing the lowest-energy levels of a given symmetry also when phonons are present. Doing so, we have found that both types of quantum phase transitions (i.e., CDW-to-CDW and CDW-to-SDW) survive a coupling of electrons to SSH phonons, but they are affected in different ways. This will be shown below by comparing relevant quantities computed with and without phonons. CDW, SDW, and BOW orderings in the ground-state of a finite (mesoscopic) system can be characterized by nonvanishing $2k_F$ correlation functions $K_{c,s,b}$, respectively.[33] These functions are defined below along with that characterizing the correlation between the BOW and lattice dimerization K_{bQ}:

$$K_{c,s}=\sum_{l=0}^{N-1}(-1)^l\langle(n_{l,\uparrow}\pm n_{l,\downarrow})(n_{0,\uparrow}\pm n_{0,\downarrow})\rangle,$$

$$K_b=\sum_{\sigma;l=0}^{N-1}(-1)^l\langle(c^\dagger_{l,\sigma}c_{l+1,\sigma}+\mathrm{H.c.})(c^\dagger_{0,\sigma}c_{1,\sigma}+\mathrm{H.c.})\rangle, \tag{2}$$

$$K_{bQ}=\sum_{\sigma;l=0}^{N-1}(-1)^{l+1}\langle(c^\dagger_{l,\sigma}c_{l+1,\sigma}+\mathrm{H.c.})Q\rangle.$$

B. Exact results for a dynamic electron-phonon coupling

To study the two quantum phase transitions, one should inspect how relevant quantities vary when crossing the critical lines by changing the model parameters. For this, we shall examine changes in nanorings driven by varying U ($U\geqslant 0$) along a fixed V line. The critical point of the c'-c transition will be denoted by U_c, that of the c-s transition, by U_s.

Let us first examine the CDW-to-CDW transition. Without phonons, $U_c/t_0=1.698$. As seen in Figs. 2(a)–2(c), for $\gamma=0$, neither K_c nor K_s is significantly affected at the c-c' transition. The jump in K_c is extremely small because the dominant correlations are of CDW type in both phases c and c'; deep inside the CDW region, K_s is anyway small. However, the K_b-curve exhibits a pronounced jump; as discussed previously,[13] the BOW correlation function is sensitive to the change of symmetry at U_c. Let us now discuss the impact of phonons. The critical point of the c-c' transition is sensitive to the electron-phonon coupling. For $\gamma=0.434$ and $\Omega/t_0=0.0656$, it is pushed downwards to $U_c/t_0=1.331$.[34] In the c' phase, the electronic correlations are practically unaffected by the coupling to phonons. There, the main effect of interactions is to renormalize the phonon frequency, but electrons and (dressed) phonons behave as separate systems. The adiabatic potential $W_0(Q)$ (i.e., the energy of the lowest eigenstate obtained by considering Q classically) is harmonic around its minimum located at $Q=0$. This holds even very close to the c-c' transition, as shown by the following example. For $V/t_0=1.2$, $\Omega/t_0=0.0656$, and $U/t_0=1.32$ ($\lesssim U_c/t_0=1.331$), the $W_0(Q)$ curvature yields a dressed phonon frequency $\tilde{\Omega}=0.7389\Omega$. Harmonic phonons with this frequency should have a ground-state average $\langle Q^2\rangle=0.5817$ and a value $\langle Q^4\rangle^{1/2}/\langle Q^2\rangle=1.7320$; these are *just* the values found by means of exact diagonalization.

Qualitatively, the effect of the c-c' transition on the BOW correlations with and without phonons is similar. In both cases, K_b curves display jumps at the corresponding critical value U_c; see Fig. 2(c). The jumps of the $K_{c,s}$ curves at c-c' transition are small in both cases [almost invisible in Figs. 2(a) and 2(b)], but a change of their slopes at $U=U_c$ can be observed in these figures in the presence of electron-phonon coupling.

Unlike in the c'-phase, phonons affect all electronic correlations in both c and s phases. In the c phase, CDW correlations are diminished by the electron-phonon coupling, while SDW correlations are enhanced. A reversed effect occurs in the s phase: SDW correlations are suppressed, whereas CDW correlations are enhanced. The electron-phonon coupling smears out the jumps in the correlation functions at the CDW-SDW transition: compare the $K_{c,s,b}$ curves with and without phonons in the region around U_s in Fig. 2. This implies that the SSH electron-phonon coupling favors the *coexistence* of CDW and SDW correlations.

Inspection of Figs. 2 shows that the ground-state lattice dimerization $\langle Q^2\rangle$ attains its maximum at the critical point U_s/t_0 (see also Sec. IV). The enhancement of the BOW correlations at the c-s transition has also been pointed out in the absence of phonons.[31,13] The K_b curves [Fig. 2(c)] show that this conclusion also holds when the electron-phonon coupling is switched on. The fact that the peaks in $\langle Q^2\rangle$ and K_b are located at the same point agrees with what one ex-

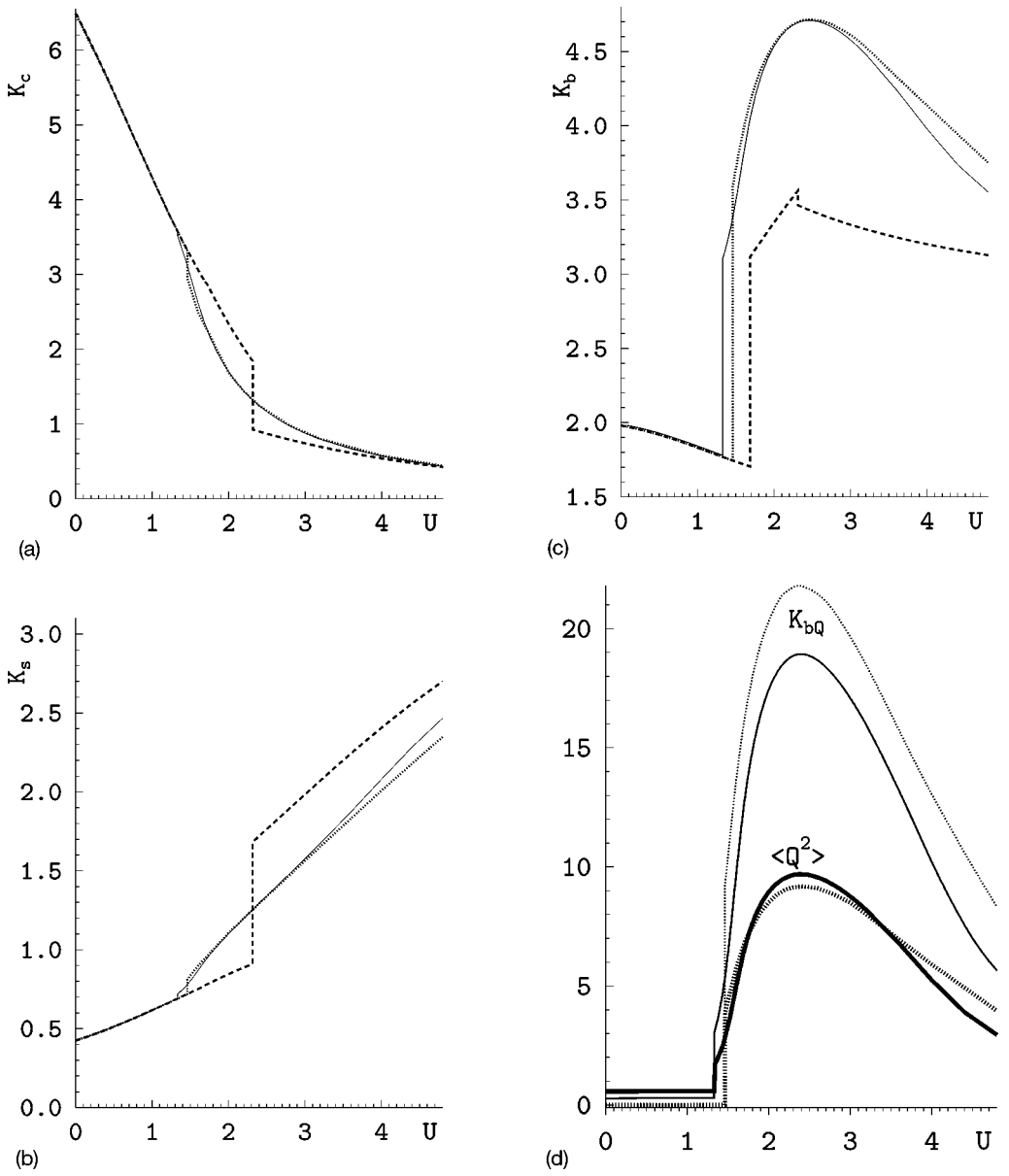

FIG. 2. CDW, SDW, BOW, and BOW-dimerization correlation functions ($K_{c,s,b,bQ}$, respectively) and mean-square dimerization $\langle Q^2 \rangle$ for 12-site periodic rings with $t_0=1$, $V=1.2$, $\Omega=0.0656$, and $\gamma=0.434$ ($U_c/t_0=1.698$, $U_s/t_0=2.310$). Solid lines: the SSH electron-phonon coupling is treated exactly (dynamically). Dotted lines: MF approximation for phonons. Dashed lines: exact calculations, but without phonons.

pects intuitively in a molecule: a shorter (longer) distance between atoms should correspond to a double (single) chemical bond. The shapes of the K_{bQ}-curves [Fig. 2(d)], with a maximum at U_s/t_0, directly confirm the correlation between the lattice dimerization and the BOW. An interesting feature visible in Figs. 2(c) and 2(d) is that both dimerization and BOW diminish more rapidly in the CDW region ($U<U_s$) than in the SDW region ($U>U_s$). The fact that the CDW is more effective than the SDW in suppressing the dimerization and the BOW can be understood intuitively within a mean-filled (MF) picture. Both CDW and BOW ordering are related to one-particle potentials with a periodicity which is twice that of the original lattice. However, the minima of the former are located *on* the lattice sites, whereas those of the latter are situated *between* adjacent sites; hence, the excess charge is located on sites in the case of a CDW, but on the bond for a BOW. Of course, the charge (summed over spin) distribution is uniform in an SDW.

The examples presented above reveal different effects of SSH phonons on the CDW-to-CDW and CDW-to-SDW transitions. The location of the critical lines is also affected in a different way. In contrast to U_c, the value of U_s is quite insensitive to phonons. For the parameter values of Fig. 2, the energies of the states *c* and *s* cross in the absence of phonons at $U_s/t_0=2.314$; for $\gamma=0.434$ and $\Omega/t_0=0.0656$, they cross at $U_s/t_0=2.310$.[34]

C. Static dimerization versus dynamic electron-phonon coupling

A popular approximation for model (1) is of the MF type, i.e., to suppose a *statically* dimerized lattice. In this section, MF results will be compared to exact ones. Besides comparison purposes, one could note that the MF approximation of the SSH-electron-phonon coupling in QD arrays can be justified, in view of the large QD mass. The inspection of Figs. 2 reveals that the MF approximation for phonons describes reasonably well certain ground-state properties. A difference between the exact and the MF results concerns the location of the c-c' transition. The higher the phonon frequency, the more is the critical value U_c shifted downwards. U_c tends to the MF-value $U_c^{MF}(=1.462t_0$ in Fig. 2) in the limit $\Omega \to 0$; for smaller frequencies ($\Omega < t_0$), the numerical results indicate that $U_c - U_c^{MF} \propto \Omega$.

The main drawback of this MF approximation is the unphysical result of a state with broken symmetry in a finite system. The symmetry can be broken only in an infinite system, but this case is less interesting here as far as phonon effects are concerned; the present model includes only a single-phonon mode, which becomes macroscopically occupied and can be treated classically. When correctly accounted for, the quantum fluctuations restore the original symmetry, and this is important, e.g., for optical absorption, as discussed below.

The MF treatment of phonons for $V=0$ in smaller dimerized clusters[22] yielded a *gradual* CDW-SDW transition. The smooth MF $K_{c,s,b,bQ}$ curves shown in Figs. 2(a)–2(d) generalizes this conclusion to the case $V \neq 0$. Although around $U=U_s$ the differences visible in Figs. 2 between the $K_{c,s,b,bQ}$-curves corresponding to a classical deformable lattice and dynamical phonons are very small, there is an important difference between the physics emerging from MF and exact treatments.[35] In the MF case, there is *no* level crossing at $U=U_s$. The smooth changes in various averaged properties simply reflect smooth changes of an approximate eigenstate whose symmetry is reduced with respect to the original one ($\mathbf{C}_{\mathcal{N},v}$, cf. Sec. II), but is nevertheless a well defined symmetry of the point group $\mathbf{C}_{\mathcal{N}/2,v}$ of a dimerized system; it does *not* change when crossing the point $U=U_s$. The qualitatively new effect brought about by the *dynamical* electron-phonon coupling is that energy levels corresponding to lowest eigenstates of different symmetries *do* cross at $U=U_s$, enabling a precise definition of a critical line $U=U_s(V)$. Quantitatively, this has only a very small impact on the curves of Fig. 2: there is a very small cusp (almost invisible in Fig. 2) in the *exact* curves at U_s, although the curves themselves remain continuous there. At higher Ω than that used in Fig. 2, the cusps become more pronounced; see Sec. IV and Figs. 4(c) and 4(d). Further physical implications of the change in symmetry at U_s will be discussed in Secs. V and VI. By contrast, at the critical point U_c there exists a level crossing even within MF.

The *lattice relaxation* is another important effect when studying electronic excitations in a mesoscopic system. Unless the exciting pulse is short with respect to the lattice relaxation time, the system in an electronically excited state will reoptimize its geometry; in general, the latter is different from the optimum geometry in the ground-state. This can be seen by inspecting the so-called adiabatic potentials $W_0(Q)$ and $W_1(Q)$, i.e., energies computed exactly at a frozen geometry Q corresponding to the electronic ground state and the lowest electronic excited state which is optically active, respectively, or by monitoring the probability distribution $P_\alpha(Q)=|\langle Q|\Psi_\alpha\rangle|^2$ to find a lattice with dimerization Q in a certain exact eigenstate $|\Psi_\alpha\rangle$ of the electron-phonon system. In Fig. 3, we present an example using parameter values deduced from reanalyzing experimental and *ab initio* data from small annulene molecules and polyacetylene.[30] The adiabatic potential $W_0(Q)$ exhibits two minima located at $Q=\pm Q_{MF}=\pm 3.296$. The probability distribution $P_0(Q)$ of the exact ground-state possesses two maxima located (roughly) at $\pm Q_{MF}$; computed quantum mechanically, their width is finite, unlike the δ-shaped maxima of the classical (MF) lattice. In contrast to the ground-state, the lowest excited electronic state which is optically active is not dimerized, as illustrated by the $W_1(Q)$ curve, possessing only one minimum at $Q=0$. Treated quantum mechanically, the lattice is nonrigid. It can and does relax: the bonds alternate in the electronic ground-state but become uniform upon a single electron-hole excitation.

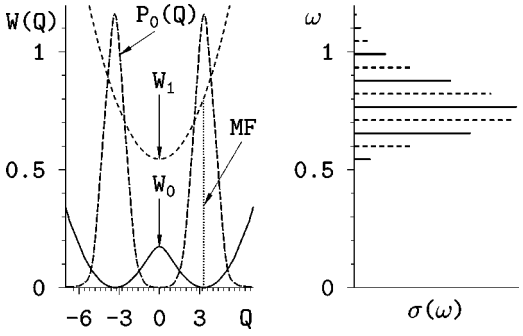

FIG. 3. Results for 12-site periodic rings and $t_0=1$, $U=1.8$, $V=0.5$, $\gamma=0.485$, and $\Omega=0.0656$. $W_{0,1}(Q)$ are the adiabatic potentials corresponding to the electronic ground-state and the lowest optically active electronic excitation, respectively, $P_0(Q)$ gives the probability to find a lattice with dimerization Q in the exact ground-state of the electron-phonon system, and $\sigma(\omega)$ is the real part of the optical conductivity. Notice the same energy scale in both right and left panels.

Summarizing, the MF approximation for phonons can satisfactorily reproduce some average ground-state properties deduced exactly. However, as discussed here and below (Sec. V) in more detail, it is totally unable to describe realistically dynamic properties of mesoscopic systems (and this, even at lower phonon frequencies), for which not only quantum fluctuations but also lattice relaxation should be appropriately considered. One should note that the lattice relaxation which is generally very important in small systems is also important for mesoscopic systems and even for polymers, because what matters is not the size of a macroscopic sample but the short conjugation length (usually several tens of units).[36]

IV. LOWEST EXCITATIONS

The electronic and lattice excitations play a key role in understanding many interesting physical properties, e.g., the

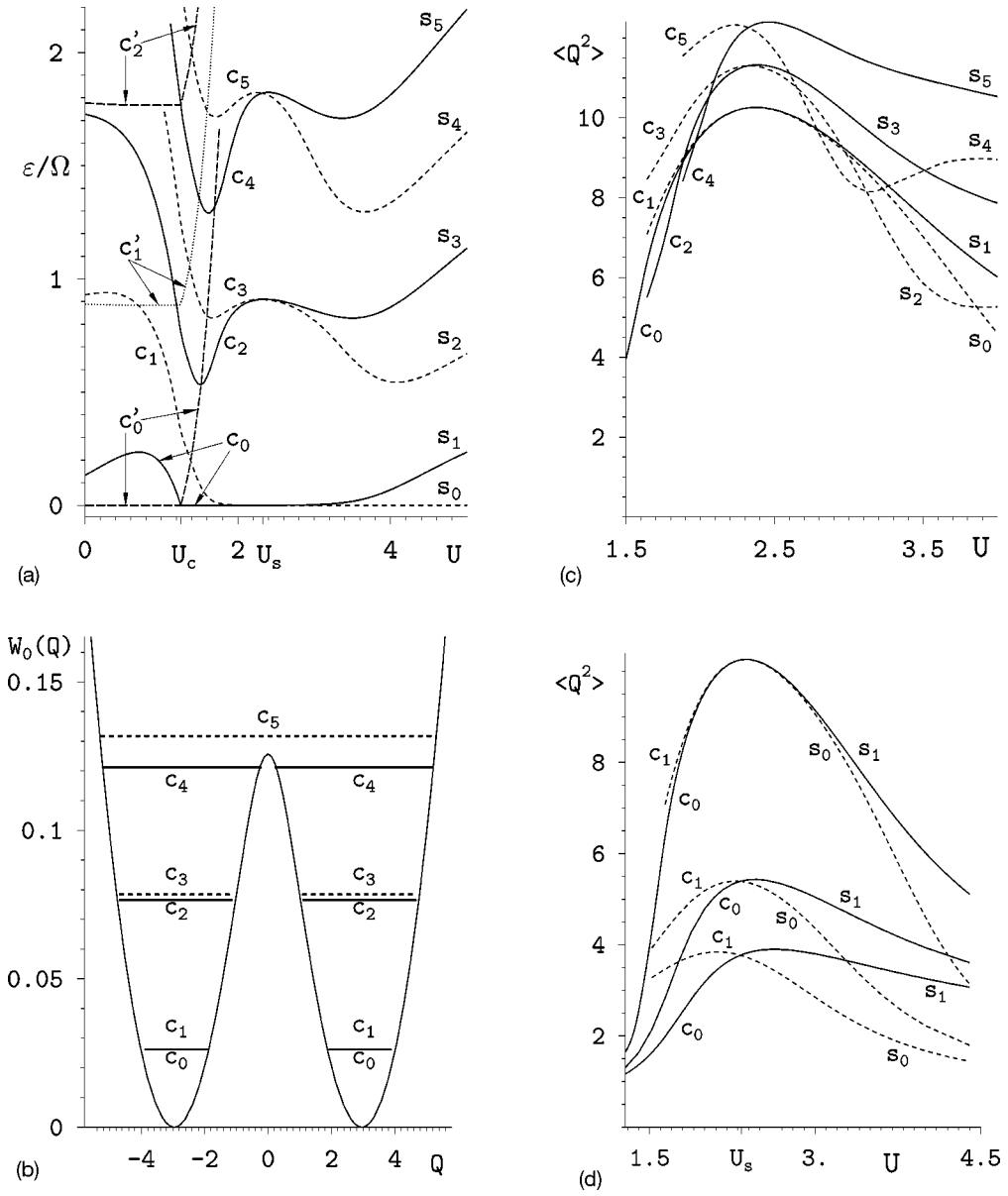

FIG. 4. U-dependent properties of 10-site antiperiodic rings at $t_0=1$, $V=1.2$, $\gamma=0.434$, and—except for the panel (d)—$\Omega=0.06$ ($U_c=1.254$, $U_s=2.322$). (a) Lowest excitation energies. Solid ($c_0\equiv s_1$, $c_2\equiv s_3$, $c_4\equiv s_5$), short-dashed ($c_1\equiv s_0$, $c_3\equiv s_2$, $c_5\equiv s_4$), long-dashed (c_0', c_2'), and dotted (c_1') lines correspond to eigenstates transforming as the one-dimensional irreducible representations of the symmetry group $^1A_1$, $^1A_2$, $^1B_1$, and $^1B_2$, respectively. See the main text for details. (b) Adiabatic potential W_0 and the energies of the lowest exact eigenstates c_0–c_5 (horizontal lines) for $U=1.92$. (The energy difference between the states c_1 and c_0 is too small to be visible within the drawing accuracy.) Mean-square lattice displacement $\langle Q^2\rangle$ for (c) the first six lowest-energy eigenstates of panel (a), and (d) the two lowest eigenstates at $\Omega/t_0=0.06$, 0.12, 0.18 (values corresponding to decreasing ordinates at $U=U_s$).

optical absorption. In Fig. 4(a), we present results for the lowest excitation energies for 10-site antiperiodic rings.[37] The physical picture emerging from the discussion of Sec. III on the ground-state is fully confirmed by the analysis of Fig. 4(a).

In Fig. 4(a), one can easily assign curves c_0', c_1', and c_2' as corresponding to the states of the c' phase with zero, one, and two harmonic vibrational quanta, respectively. These curves are equidistant and horizontal for $U<U_c$, where the ground-state is a c' phase. Above U_c they are no more horizontal, because the ground-state is now of c-type, but the energy differences remain practically U independent. This agrees with the conclusion of Sec. III: the c' phase consists of two (practically) decoupled subsystems (electrons and harmonic phonons).

The curves c_0 and s_0 correspond to the lowest-energy states with the symmetry of the c and s phases, respectively. The former is the ground-state for $U_c<U<U_s$ and the latter for $U>U_s$. Being of different symmetries, these two levels can and do cross at $U=U_s$ (no avoiding crossing). The c_0 level extends within the region $U>U_s$ as the lowest excitation s_1 in the s phase. A similar behavior is encountered for

excited states: the c_k level (kth excitation in the c phase) crosses at $U=U_s$ with the s_k level (kth excitation in the s phase). The s_{k+1} level represents the smooth continuation of the c_k-level with the same symmetry into the s phase ($U>U_s$); for $U<U_s$, one should interchange the level labels ($s \rightleftharpoons c$) in the above statement. Within an adiabatic description,[17,18] one would assign, e.g., the s_0 level as the ground-state for both electrons and lattice in the s region, while the s_k state would be the product of the electronic ground state and the kth lattice excitation.

Figure 4(a) also reveals that, close to the point U_s and far apart from it, the excitations have a *different* physical meaning on either side of the transition. Sufficiently far away from U_s, the energy spacing between adjacent excitations (c_{k+1} and c_k for $U_c<U \ll U_s$ or s_{k+1} and s_k for $U \gg U_s$) is nearly constant. There, these excitations can be ascribed to normal, nearly harmonic phonons of a weakly dimerized system [cf. Figs. 2(d) and 4(a)]. On the contrary, in the dimerized regime ($U \approx U_s$), the excitations can be ordered in pairs, each pair consisting of two almost degenerate tunnel partners of different symmetry, see Fig. 4(a).

We shall present below a number of arguments confirming this interpretation in terms of a tunnel effect in a symmetric double well potential $W_0(+Q)=W_0(-Q)$. The lowest-energy of a classic object in this potential corresponds to two states $Q=+Q_{MF}$ and $Q=-Q_{MF}$ which are equivalent. Instead of a twofold degenerate ground-state, the two lowest energy eigenstates of a quantum oscillator moving in the potential $W_0(Q)$ can be (approximately) expressed as the symmetric and antisymmetric superpositions of two wave packets centered on $+Q_{MF}$ and $-Q_{MF}$. Unlike in the classical case, they are no more degenerate. The small difference ε of their energies is the result of the quantum tunneling across an energy barrier $E_B=W_0(0)-W_0(Q_{MF})$ over a distance $\sim 2u_0 \sim \hbar Q_{MF}/\sqrt{NM\Omega}$ [cf. Figs. 3 and 4(b)]. If the barrier is sufficiently high, one can estimate the tunnel splitting energy ε semiclassically; it decreases exponentially with the quantity $u_0\sqrt{E_B m}/\hbar \propto z\sqrt{m/M}$, where m is the oscillator mass and $z \equiv \Delta_{MF}\sqrt{E_B/t_0}/(\gamma\Omega)$. In Fig. 5(a), we have plotted the quantity z against the lowest excitation energy $\varepsilon=|E(c_0)-E(s_0)|$ computed exactly. To get the curves of Fig. 5(a), U has been varied in the ranges where ε is small, and this *both* in the CDW and in the SDW region [$1.6 \lesssim U/t_0 \lesssim 2.2$ and $2.5 \lesssim U/t_0 \lesssim 4$, cf. Fig. 4(a)]. In both regions we found that the curves $\log\varepsilon$ versus z are linear [cf. Fig. 5(a)] to a very good approximation; furthermore, for a given size N, one cannot distinguish the curve corresponding to U values in the CDW region from that corresponding to U values in the SDW region. So, the exact quantity ε behaves just as one expects for a tunnel splitting energy.

This is a strong evidence for the tunnel effect, but this is not the whole issue. As seen in Fig. 5(a), the curves for z are linear, but they do depend on N. In view of the above considerations, one should immediately rule out a one-particle origin of the tunneling: if the tunnel effect were of single-particle origin, m would be N independent and the z curves would be N independent. By contrast, the curves for $z\sqrt{N}$ are (almost) N independent. The fact that not the z curves, but

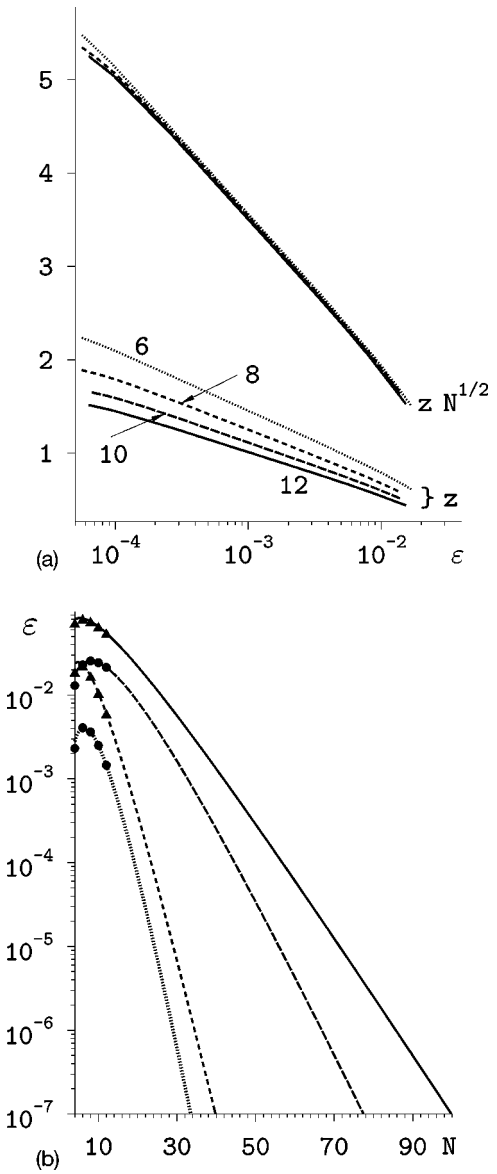

FIG. 5. (a) Curves for $z \equiv \Delta_{MF}\sqrt{E_B/t_0}/(\gamma\Omega)$ and $z\sqrt{N}$ plotted vs. the exact lowest excitation energy ε for several sizes N. The N values are indicated on the z-curves, but are omitted for the $z\sqrt{N}$ curves, because the latter are practically N independent [$E_B \equiv W_0(0)-W_0(Q_{MF})$]. (b) The size dependence of the lowest excitation energy ε. The lines have been deduced by fitting the points (exact numerical results) allowing for logarithmic corrections to the energy barrier (see main text). Solid, long-dashed, short-dashed, and dotted lines correspond to $(U,\gamma)=(5.0,0.434)$, (4.2, 0.434), (5.0, 0.560), and (4.2, 0.560), respectively. The other parameter values are $t_0=1$, $V=2$, and $\Omega=0.25$.

the $z\sqrt{N}$ curves are N independent implies $m \propto N$, i.e., a *collective* tunneling occurs. Concerning the N dependence, a comment is still in order. Above, we have discussed the dependence of ε on N indirectly, by means of the barrier $E_B(N)$. In an extended solid one expects $\Delta_{MF}=\text{const}$ and $E_B(N) \propto N$, because the former is an intensive quantity (the gap parameter) while the latter an extensive one (energy gain due to dimerization). Accordingly, ε should fall off exponen-

tially at sufficiently large sizes. However, at the sizes for which the numerical diagonalization can be done, this exponential decrease can be seen only in parameter ranges where the dimerization is very favorable, i.e., for sufficiently strong electron-phonon coupling and close enough to the point $U=U_s$; otherwise, at small sizes logarithmic corrections to the energy barrier become important. This is illustrated in Fig. 5(b).

Trivially, in the two degenerate states of a classical lattice ($\Omega \to 0$) the mean-square lattice displacement is the same: $(+Q_{MF})^2=(-Q_{MF})^2$. Except for the critical point $U=U_s$, the two lowest-energy eigenstates—(c_0, c_1) or (s_0, s_1)—are characterized by different $\langle Q^2\rangle$ (as well as other average properties such as K_{bQ}). These differences are the larger, the farther one moves from the critical point $U=U_s$ and/or the larger is the frequency Ω. This behavior is illustrated by the Figs. 4(c) and 4(d), respectively. Notice that the higher the phonon frequency, the more shifted in opposite directions the curves appear corresponding to these two states. In the ground-state the largest values of $\langle Q^2\rangle$ and K_{bQ} correspond to $U=U_s$, but their maxima for the state c_0 (s_0) are reached at $U \gtrsim U_s$ ($U \lesssim U_s$).

Above, we have provided arguments on a (collective) tunnel effect by only referring to the two lowest eigenstates. The inspection of higher excitations gives further support for tunneling. In accord with the idea of the tunneling in a double-well potential [Fig. 4(b)], the energy splitting of the tunnel partners (c_0, c_1), (c_2, c_3), (c_4, c_5), ... for $U \lesssim U_s$, and (s_0, s_1), (s_2, s_3), (s_4, s_5), ... for $U \gtrsim U_s$ becomes larger for higher excitations. This is clearly visible in Fig. 4(a): $\varepsilon(c_1)-\varepsilon(c_0)<\varepsilon(c_3)-\varepsilon(c_2)<\varepsilon(c_5)-\varepsilon(c_4)$ and $\varepsilon(s_1)-\varepsilon(s_0)<\varepsilon(s_3)-\varepsilon(s_2)<\varepsilon(s_5)-\varepsilon(s_4)$ at, say, $U/t_0=1.8$ and $U/t_0=2.5$, respectively. Also, average properties such as $\langle Q^2\rangle$ are more different for tunnel partner states of higher energy; see Fig. 4(c).

The above results can be rephrased more physically in the language of molecular physics. In the coupled electron-phonon system, a coherent tunneling occurs between two states that are classically equivalent, $\cdots X\text{—}X\text{=}X\text{—}X\text{=}\cdots$ and $\cdots X\text{=}X\text{—}X\text{=}X\text{—}\cdots$. Here, $X\text{=}X$ ($X\text{—}X$) means a double (single) bond, i.e., a shorter (longer) interatomic distance *and* almost two (no) electrons between adjacent atoms X in the ring. This is a collective tunneling to which *all* electrons as well as phonons contribute. These results generalize earlier findings for systems where either electron-electron or electron-phonon interaction is absent.[18,13] In view of the role played by the tunnel effect it is also clear why, from the present standpoint, mesoscopic systems are more interesting than macroscopic ones. According to the physics underlying Figs. 5(a) and 5(b), the energy separation of the states c_0 and s_0 becomes vanishingly small in infinite systems. Instead of a well-defined c-s critical line separating two distinct c and s phases of a mesoscopic system, a macroscopic system is characterized by a twofold degenerate ground-state and there is no quantum phase transition.

For later purposes, it is worth noting that, in all phases (c', c, s), every second excitation has the same symmetry; e.g., the states $\{s_{2k}\}_{k\geq 0}$ have the same symmetry, which differs from the unique symmetry of the set $\{s_{2k+1}\}_{k\geq 0}$. The symmetries of s_k and $c_{k\pm 1}$ are identical.

V. OPTICAL ABSORPTION

The smooth changes of the correlation functions $K_{c,s,b,bQ}$ and lattice dimerization $\langle Q^2\rangle$ around $U=U_s\approx 2V$ discussed in Sec. III might suggest that a critical point of the CDW-SDW transition can by defined only by some arbitrary convention. However, the contrary is true. As illustrated in the example of Sec. IV, our exact numerical results show that levels corresponding to the lowest energies with different symmetries transforming according to the one-dimensional irreducible representations of the symmetry group $\mathbf{C}_{\mathcal{N},v}$ do cross at a definite point $U=U_s\lesssim 2V$ for given t_0 and V, i.e., the ground-state symmetry does change there. To demonstrate that this fact is also of practical interest, one should consider properties sensitive to symmetry changes. The optical absorption is quite suitable for this purpose, as revealed below by the results on the real part of the optical conductivity $\sigma(\omega)$.

We present results for $\sigma(\omega)$ at two U values, one slightly smaller [Fig. 6(a)] and the other slightly greater [Fig. 6(b)] than U_s. Spectral lines corresponding to optical absorption both in the ground-state and in the lowest excited state (solid and dashed lines, respectively) are shown there. By comparing the spectral lines related to optical transitions from the ground-state to those from the first excited state of Figs. 6(a) and 6(b), one can see that their ordering becomes reversed when crossing the critical point $U=U_s$. To understand this, one should remember the fact that levels cross at $U=U_s$. Close enough to U_s [cf. Sec. IV and Fig. 4(a)],[38] the ground (first excited) state s_0 (s_1) for $U>U_s$ has the same symmetry as the first excited state (ground-state) c_1 (c_0) for $U<U_s$.[39] In view of their different symmetries, transitions allowed optically from the state c_0 (or s_1) become forbidden from the state c_1 (or s_0) and vice versa. Possible implications of this behavior will be discussed in Sec. VI.

To discuss the physical origin of the absorption lines of Fig. 6, we shall return to Fig. 3. In a *rigid* dimerized lattice, characterized by δ-shaped probability distributions $P(Q)$, the lowest electronic excitation increases the energy of the system by $\omega_{max}=W_1(Q_{MF})-W_0(Q_{MF})$.[40] This process, indicated in Fig. 3 by the vertical dotted line, gives rise to a single spectral line in the optical absorption at the frequency $\omega=\omega_{max}$. By contrast, the absorption spectrum computed quantum mechanically $\sigma(\omega)$ consists of several (almost) equidistant spectral lines. In the right panel of Fig. 3, the solid lines represent the absorption spectrum in the ground-state s_0, whereas the dashed ones correspond to absorption processes in the lowest excited state s_1. Although the maximum of the two absorption spectra is roughly located at the MF frequency ω_{max}, the exact spectra exhibit a rich structure (of phononic origin, see below) which is completely absent in the MF picture. One can get physical insight into the optical absorption by comparing the right and left panels of Fig. 3. Because of quantum fluctuations, phonon wave packets have a finite extension [$P(Q)$'s are not δ functions] and an absorption process can bring the system from the

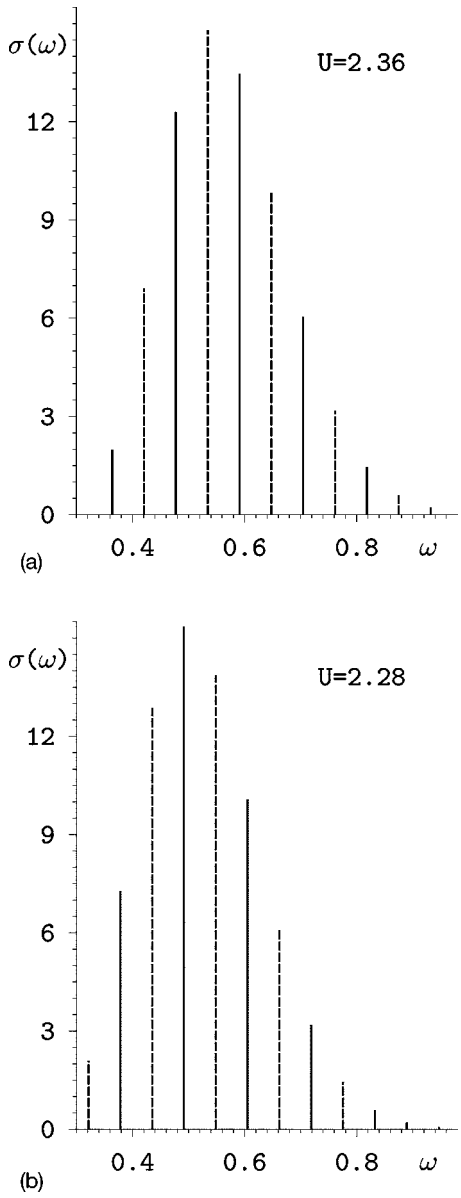

FIG. 6. The real part of the optical conductivity $\sigma(\omega)$ computed in the electron-phonon ground-state and its tunneling partner (solid and dashed lines, respectively) for 12-site periodic rings with $t_0=1$, $V=1.2$, $\Omega=0.0656$, $\gamma=0.434$ and (a) $U=2.28$ ($<U_s=2.310$) and (b) $U=2.36$ ($>U_s=2.310$). Note the reversed roles of the solid and dashed lines around U_s.

minimum energy $W_0(Q_{MF})$ to an energy $W_1(Q)$ with a certain Q-dependent probability.

In Fig. 3, the first spectral line, which belongs to the optical spectrum in the ground-state s_0, has a frequency $\omega_{th}=0.54360$, extremely close to the lowest possible energy difference $\omega_{th}^{cl}\equiv \min_Q W_1(Q)-W_0(Q_{MF})=W_1(0)-W_0(Q_{MF})=0.543\,55$.[41] The next lines of the *ground-state* spectrum (solid lines in Fig. 3) are practically equidistant; the separation is $\delta\omega=0.1112$. This is related to the fact that the harmonic approximation with a phonon frequency $\Omega_1=0.0556$ yields a curve indistinguishable from the $W_1(Q)$-curve within the drawing accuracy of Fig. 3; notice that $\Omega_1=\delta\omega/2$ and remember that, for a harmonic oscillator, every second eigenstate possesses the same parity, while every two successive eigenstates are of opposite parity. The optical spectrum of the ground-state s_0 comprises contributions of even-order overtones (see also Sec. IV); because of symmetry, odd-order overtones are suppressed. But just for the same reasons, odd-order overtones contribute to the spectrum in the lowest excited state s_1, whereas those of even order are suppressed. Accordingly, the inspection of the right panel of Fig. 3 reveals that a spectral line belonging to the s_0 spectrum is located symmetrically between two adjacent lines of the s_1 spectrum and vice versa. The tunnel splitting energy $E(s_1)-E(s_0)=2.5\times10^{-5}\,t_0$ is too small to play a role within the drawing accuracy of Fig. 3.

In the above analysis of the optical absorption of Fig. 6, we have focused our attention on the CDW-SDW transition to illustrate that, although certain properties vary smoothly (cf. Sec. III), there also exist physical quantities exhibiting jumps at the corresponding critical point. For a similar reason, quantities related to optical absorption also display jumps at the CDW-to-CDW transition, as demonstrated previously even without phonons.[13]

VI. SUMMARY AND OUTLOOK

The results reported in this paper demonstrate that systems with mesoscopic sizes described by an extended Hubbard-SSH model exhibit properties which are even more interesting than those of infinite ones. The main differences are related to the fact that the symmetry of the ground-state can change when crossing certain critical lines in the space of model parameters. As demonstrated previously in the absence of phonons,[13] for $V>0$, the phase diagram of mesoscopic systems comprises (i) CDW-SDW and (ii) CDW-CDW critical lines. They define quantum phase transitions between states characterized by (i) different types of correlations and symmetries and (ii) states possessing the same type of correlations but different symmetries, respectively. We have shown here that these two kinds of quantum phase transitions survive if electrons are coupled to SSH phonons, but they are affected in different ways. The location of the CDW-CDW critical point exhibits a significant dependence on both electron-phonon coupling and phonon frequency, while that of the CDW-SDW critical point is little affected by SSH phonons. Discontinuities in the values and/or the slopes of relevant correlation functions characterize the CDW-to-CDW transition both with and without SSH electron-phonon coupling. In contrast to this, the SSH-electron-phonon coupling smears out the jumps present in the absence of phonons at the CDW-SDW transition; it makes a CDW-SDW coexistence possible.

Our calculations confirm and generalize a number of previous findings related to the CDW-SDW transition obtained in previous exact numerical diagonalization studies in the absence of phonons,[22,31,13] or by treating the lattice as a classical deformable object:[22] for example, the enhancement of the BOW correlations and lattice dimerization. Since we are mainly interested in finite systems, we only note below several aspects brought about by the electron-phonon coupling which are relevant for infinite systems as well.

The electron-electron interaction can substantially modify the dimerization and the CDW, SDW, and BOW correlation functions. In Fig. 2(d), we present a situation where, sufficiently close to (farther from) the point $U=U_s$, the dimerization is larger (smaller) than that for $U=V=0$.[42] This is the case if the electron-phonon coupling is weak enough. For stronger electron-phonon coupling, $\gamma>\gamma_{cr}$, $\langle Q^2\rangle|_{U=V=0}$ becomes larger than $\langle Q^2\rangle$ for all U-values. For $N=12$, $V/t_0=1.2$, and $\Omega/t_0=1$, we found $\gamma_{cr}=0.880$; its MF counterpart (i.e., $Q^2_{MF}|_{U=V=0}\rangle Q^2_{MF}$ for any U) is $\gamma>\gamma_{cr}^{MF}=0.867$. The question whether the dimerization is enhanced or not by Hubbard-type interactions represents a subject of interest. Earlier studies on infinite systems agreed about the following qualitative behavior: as U increases from zero, the dimerization first increases, attains a maximum and then decreases; see, e.g., the discussion in Ref. 22. Extrapolations of the results deduced by exact numerical diagonalization for a classical lattice have been employed to investigate the influence of U on the dimerization in infinite systems for $V=0$.[22] They gave support for the aforementioned behavior only for sufficiently weak electron-phonon coupling. Although we shall not consider this issue, we mention that an argument invoked to this aim in Ref. 22 was that the curves[43] of the dimensionless MF dimerization $x_{MF}(U)$ for different N values pass through an N-independent point U_0. By treating the electron-phonon coupling *dynamically*, we found that this is no longer true. Therefore, the problem should merit reconsideration, particularly at higher phonon frequencies, where this effect turned out to be more pronounced.

The optical conductivity examined here in conjunction with symmetry changes at critical lines also served to reveal the important part played by lattice relaxation. As shown in Fig. 3 and previously in the absence of electron-electron interaction,[17] the tail of the *exact* absorption curve, penetrating into the MF optical gap, is directly related to lattice relaxation. Recent studies on optical properties investigated larger one-dimensional systems within DMRG,[44] accounting (almost) exactly for strong electronic correlations but considering a frozen lattice (eventually at optimized ground-state geometry), i.e., making use of the approximation usually called ''adiabatic.''[45] The present results for $\sigma(\omega)$ demonstrate that this approximation is unable to describe the optical smearing in finite systems. To treat appropriately this phenomenon in larger systems, the DMRG calculations should include dynamic electron-phonon couplings rather than classical frozen lattices.

The issues noted above indicate several significant effects of quantum phonon fluctuations, but other effects are even more interesting. There is an important difference between the exact and MF treatments: the ground-state symmetry does change in the former case, while in the latter there is *no* level crossing at $U=U_s$ (cf. Sec. III C). To demonstrate that a critical phenomenon really occurs at $U=U_s$, one can monitor a physical property sensitive to symmetry changes, such as optical absorption. To exemplify, we have shown the jump in the lowest absorption frequency in the ground state when crossing the critical point $U=U_s$ (cf. Fig. 6). If the temperature is sufficiently low ($T\sim 0.01$ K for the parameters of Fig. 3), only the ground-state is populated. Then, by varying model parameters in a controlled way, one can cross the critical point U_s, and this will result in a jump in the absorption onset. For the values employed in Fig. 6, the lowest absorption frequency in the ground-state will be suddenly redshifted by $\Delta\omega/t_0=0.0567$ at $U=U_s$ by increasing U. Another possibility would be to prepare a system, e.g., with $U\lesssim U_s$: at sufficiently low temperatures $[k_BT<E(c_1)-E(c_0)]$, only optical transitions from the ground state c_0 can occur, while at higher temperatures $[k_BT>E(c_1)-E(c_0)]$, the state c_1 becomes also populated and the transitions from this state will shift the absorption spectrum toward the red; for illustration, compare the position of the first dashed and solid lines in Fig. 6.

We have found[30] that the extended Hubbard-SSH model is able to describe quantitatively a variety of properties of smaller ring-shaped C_NH_N molecules (benzene, cyclooctatetraene, cyclobutadiene); moreover, extrapolations to larger sizes of these exact results reasonably agree with data in polyacetylene. However, these systems turned out to be too far from the critical points. We could not find more suitable candidates among existing molecular rings closer to the points $U=U_{c,s}$ where the most interesting phenomena discussed above occur. Nanorings of QD's are much more promising. Advances in nanotechnologies allow to tune model parameters, and hence, to explore extended regions of the phase diagram comprising critical lines. For $D/(2R)=1.107$, the classical approximation predicts $u/v=2$ [Fig. 1(b)], a situation close to the CDW-SDW critical line. While this is only a crude estimate,[46] the interesting results found here could encourage experimental efforts for searching a CDW-SDW transition in nanorings of QD's sufficiently close to each other. For the state-of-the-art of nanosciences, a *perfectly* regular array of *identical* QD's represents a too idealized picture. Therefore, the inclusion of disorder in the theoretical model remains a desirable step.

ACKNOWLEDGMENT

I.B. wishes to thank for the financial support of this work provided by the Sonderforschungsbereich Grant No. 195 at the Universität Karlsruhe and the Fonds der Chemischen Industrie.

*Permanent address: National Institute for Lasers, Plasmas and Radiation Physics, ISS, RO-76900 Bucharest-Măgurele, Romania. Email address: ioan@pci.uni-heidelberg.de

[1] *The Hubbard Model*, edited by D. Baeriswyl, D. K. Campbell, and J. M. P. Carmel (Plenum Press, New York, 1995).

[2] *Density-Matrix Renormalization—A New Numerical Method in Physics*, edited by I. Peschel, X. Wang, M. Kaulke, and K. Hallberg, Lecture Notes in Physics Series, Vol. XVI (Springer-Verlag, Berlin, 1999).

[3] E. Fradkin and J.E. Hirsch, Phys. Rev. B **27**, 1680 (1983).

[4] M.A. Kastner, Phys. Today **46** No. 1, 24 (1996).

[5] J.R. Heath, C.M. Knobler, and D.V. Leff, J. Phys. Chem. B **101**, 189 (1997); C.P. Collier, R.J. Saykally, J.J. Shiang, S.E. Henrichs, and J.R. Heath, Science **277**, 1978 (1997); G. Markovich,

C.P. Collier, and J.R. Heath, Phys. Rev. Lett. **80**, 3807 (1998).
[6] J.J. Shiang, J.R. Heath, C.P. Collier, and R.J. Saykally, J. Phys. Chem. B **102**, 3425 (1998).
[7] G. Medeiros-Ribeiro, D.A.A. Ohlberg, R.S. Williams, and J.R. Heath, Phys. Rev. B **59**, 1633 (1999).
[8] N. Herron, J.C. Calabreses, W.E. Farneth, and Y. Wang, Science **259**, 1426 (1993); A.P. Alivisatos, *ibid.* **271**, 933 (1996).
[9] L. Kouvenhoven, Science **268**, 1440 (1995); R.H. Blick, R.J. Haug, J. Weis, D. Pfannkuche, K. von Klitzing, and K. Erbel, Phys. Rev. B **53**, 7899 (1996); C. Livermore, C.H. Crouch, R.M. Westerveld, K.L. Kampman, and A.C. Gossard, Science **274**, 1332 (1996); T.H. Oosterkamp, T. Fujisawa, W.G.v.d. Wiel, K. Ishibashi, R.V. Hijman, S. Tarucha, and L. Kouvenhoven, Nature (London) **395**, 873 (1998).
[10] C.A. Stafford and S. Das Sarma, Phys. Rev. Lett. **72**, 3590 (1994); C.A. Stafford, R. Kotlyar, and S. Das Sarma, Phys. Rev. B **58**, 7091 (1998); Z. Yu, A.T. Johnson, and T. Heinzel, *ibid.* **58**, 13830 (1998).
[11] F. Remacle and R.D. Levine, J. Am. Chem. Soc. **122**, 4048 (2000); F. Remacle, Habilitation Thesis, Université de Liège, 2001.
[12] I. Bâldea and L.S. Cederbaum, Phys. Rev. Lett. **89**, 133003 (2002).
[13] I. Bâldea, H. Köppel, and L.S. Cederbaum, Solid State Commun. **115**, 593 (2000); Phys. Rev. B **63**, 155308 (2001); Eur. Phys. J. B **20**, 289 (2001).
[14] W.P. Su, J.R. Schrieffer, and A.J. Heeger, Phys. Rev. Lett. **42**, 1698 (1979); Phys. Rev. B **22**, 2099 (1980).
[15] L. Salem, *The Molecular Orbital Theory of Conjugated Systems* (Benjamin, New York, 1966).
[16] G.-P. Borghi, A. Girlando, A. Painelli, and J. Voigt, Europhys. Lett. **34**, 127 (1996); A. Dobry, A. Greco, S. Koval, and J. Riera, Phys. Rev. B **52**, 13 722 (1996).
[17] I. Bâldea, H. Köppel, and L.S. Cederbaum, Phys. Rev. B **55**, 1481 (1997).
[18] I. Bâldea, H. Köppel, and L.S. Cederbaum, Solid State Commun. **106**, 733 (1998); Eur. Phys. J. B **3**, 507 (1998); Phys. Rev. B **60**, 6646 (1999).
[19] A.W. Sandvik, R.R.P. Singh, and D.K. Campbell, Phys. Rev. B **56**, 14 510 (1997); D. Augier, D. Poilblanc, E. Sø rensen, and I. Affleck, *ibid.* **58**, 9110 (1998); G. Wellein, H. Fehske, and A.P. Kampf, Phys. Rev. Lett. **81**, 3956 (1998).
[20] L.G. Caron and S. Moukouri, Phys. Rev. B **56**, R8471 (1997); E. Jeckelmann and S.R. White, *ibid.* **57**, 6376 (1998); C. Zhang, E. Jeckelmann, and S.R. White, *ibid.* **60**, 14092 (1999); E. Jeckelmann, C. Zhang, and S.R. White, *ibid.* **60**, 7950 (1999).
[21] Anti periodic rings might be unphysical. Therefore, one should remember that periodic rings enclosing an Aharonov-Bohm magnetic flux $\phi/2$ ($\phi=hc/e$) are equivalent to antiperiodic rings in zero flux; see, e.g., Ref. 18, and references cited therein.
[22] V. Waas, H. Büttner, and J. Voit, Phys. Rev. B **41**, 9366 (1990).
[23] B. Nathanson, O. Entin-Wohlman, and B. Mühlschlegel, Phys. Rev. B **45**, 3499 (1992).
[24] One should note that such open-shell clusters are exactly equivalent to *extended* periodic systems where the Brillouin-zone sampling is restricted to N points and includes the Fermi points (so-called small-crystal approach); see R.H. Victora and L.M. Falicov, Phys. Rev. Lett. **55**, 1140 (1985); E.C. Sowa and L.M. Falicov, Phys. Rev. B **35**, 3765 (1987).
[25] C.-L. Wang, W.-Z. Wang, G.-L. Gu, Z.-B. Su, and Lu Yu, Phys. Rev. B **48**, 10 788 (1993).
[26] For metallic dots prepared by Heath's group, (Refs. 5 and 6 ε is the dielectric constant of the alkane chains of the ligands that stabilize the metallic core ($\varepsilon_r \simeq 2-3$), and typical U values are of a few tenths of eV, determining an energy scale much larger than thermic energies even at room temperature. For semiconducting dots with comparable sizes, because ε is larger (for GaAs, $\varepsilon_r \simeq 13$), U can be of the order of tens of meV.
[27] F. Remacle, C.P. Collier, G. Markovich, J.R. Heath, and U. Banin, J. Phys. Chem. B **102**, 7727 (1998).
[28] W. B. Smythe, *Static and Dynamic Electricity* (McGraw-Hill, New York, 1968), p. 131.
[29] R. G. Parr, *Quantum Theory of Molecular Electronic Structure* (Benjamin, New York, 1963).
[30] I. Bâldea (unpublished).
[31] M. Nakamura, J. Phys. Soc. Jpn. **68**, 3123 (1999); Phys. Rev. B **61**, 16 377 (2000).
[32] In the present discussion of the 12-site nanoring, we have mentioned the states c, c', and s, since these are the types of ground-states possible in the case $V>0$, to which we have restricted ourselves. A complete discussion of the ground state is given in Ref. 13.
[33] Within a MF picture, a certain ordered state is characterized by an order parameter, i.e., a nonvanishing average of an appropriate operator. For a CDW, one can use the amplitude of the modulated electron density, i.e., the nonvanishing site-independent average $(-1)^l\langle(n_{l,\uparrow}-1/2)+(n_{l,\downarrow}-1/2)\rangle$. This means that, e.g., the charge excess at each even-numbered site is equal to the charge deficit at each odd-numbered site. Since there is another equivalent configuration (obtained by interchanging the words even and odd above), the aforementioned average vanishes in the ground-state computed quantum mechanically because of the tunneling between two equivalent configurations. Therefore, order parameters cannot be employed to characterize orderings in finite (mesoscopic) systems, and one should use correlation functions instead.
[34] The changes in the critical points for antiperiodic 10-site rings are similar. At $V/t_0=1.2$, we get in the absence of phonons $U_s/t_0=2.321$ and $U_c/t_0=1.608$. In the presence of SSH-phonons with $\gamma=0.434$ and $\Omega/t_0=0.06$ ($\Omega/t_0=0.0656$), the corresponding values are $U_s/t_0=2.322(2.322)$ and $U_c/t_0=1.254(1.239)$. The only difference between the phase diagram of 12-site periodic rings and 10-site antiperiodic rings is that, in the latter case, the phase s has the symmetries of the antisymmetric superposition $|\mathrm{SDW}_1\rangle-|\mathrm{SDW}_2\rangle$; for details, see the last part of Ref. 13.
[35] The MF curve for K_b shown in Fig. 2(c) has been obtained by averaging the BOW correlation functions over the two equilibrium geometries $Q=+Q_{MF}$ and $Q=-Q_{MF}$ which are classically equivalent.
[36] R. Silbey, in *Conjugated Polymers and Related Materials*, edited by W. R. Salaneck *et al.* (Oxford University Press, Oxford 1993).
[37] As already noted (Ref. 34), there are no significant differences between 10-site antiperiodic rings and 12-site periodic rings.
[38] This is no longer the case for U values more distant from U_s, because of the interplay between phononic and electronic excitations. For instance [cf. Fig. 4(a)], the lowest excitation c_0' at $U \gtrsim U_c$ is of electronic nature. Within an adiabatic description,

(Ref. 18) c_0' would be the product of the lowest excited electronic state and the phononic ground-state.

[39] This is also the reason why the sequence of spectral lines of Figs. 3 and 6(b) is the same: in both cases, $U > U_s$.

[40] In agreement with the well-known Franck-Condon principle, the present calculations show that the absorption maximum corresponds to the vertical transition (i.e., at the same value $Q = Q_{MF}$) between adiabatic potentials.

[41] Even this small difference between ω_{th} and ω_{th}^{cl} can be quantitatively explained by accounting for the zero-point vibrational energies deduced from the slightly different curvatures of $W_0(Q)$ and $W_1(Q)$ at $Q = Q_{MF}$ and $Q = 0$, respectively.

[42] To see this, one should compare the curves of Fig. 2 with the values obtained by setting $U = V = 0$. Within the exact treatment, we get $K_b = 3.526$, $\langle Q^2 \rangle = 6.903$, and $K_{bQ} = 13.196$. Within MF, the values are $K_{b,MF} = 3.521$, $Q_{MF}^2 = 6.344$, and $K_{bQ,MF} = 12.965$.

[43] The dynamical counterpart x of the dimensionless MF dimerization $x_{MF} \equiv 2u_0\sqrt{K/t_0} = Q_{MF}\sqrt{\Omega}/\sqrt{Nt_0}$ is $[\langle Q^2 \rangle - \Omega/(2\tilde{\Omega})]^{1/2}\sqrt{\Omega}/\sqrt{Nt_0}$.

[44] W.P. Su and G.Z. Wen, Synth. Met. **85**, 1041 (1996); Z. Suhai, J.L. Brédas, A. Saxena, and A.R. Bishop, J. Chem. Phys. **109**, 2549 (1998); S. Nishimoto, M. Takahashi, and Y. Ohta, J. Phys. Soc. Jpn. **69**, 1594 (2000).

[45] For a discussion of various adiabatic approximations, see I. Bâldea, H. Köppel, and L.S. Cederbaum, J. Phys. Soc. Jpn. **68**, 1954 (1999).

[46] Straightforward calculations using the values of Ref. 6 and 7 show that, while remarkably reproducing basic experimental findings, the classical model of spherical dots is only able to estimate U up to a factor of the order of unity.